Ocean Surface Current Inversion Method for a Doppler Scatterometer

Qingliu Bao, Mingsen Lin, Youguang Zhang, Xiaolong Dong, Shuyan Lang, and Peng Gong

***Abstract*— The ocean surface current is a very important parameter of ocean dynamic environment. It is connected to global climate change, marine environment forecasting, marine navigation, engineering security, and so on. The observation and prediction of ocean surface current have attracted more and more concern. Doppler Scatterometer (DopScat) is a new type of radar for ocean surface wind and current field remote sensing. The ocean surface current inversion method of DopScat impacts the measurement accuracy directly. In this paper, we establish the simulation model of a DopScat and provide the radial velocity error model. The numerical ocean surface Doppler spectrum model is also introduced and validated with the empirical geophysical model function in C-band (CDOP). The suitable ocean wave elevation spectrum and directional distribution function are selected. What is more, this paper establishes the maximum likelihood estimation (MLE) method to retrieve the ocean surface current and wind simultaneously. The retrieval accuracy for different positions in cross track, different wind speeds, and different current speeds are analyzed. At last, the global ocean current field is observed by DopScat and the ocean current is retrieved. In our simulation, the orbit parameters and observation geometry of DopScat are the same as that of HY-2A scatterometer. The retrieval results show that global current speed standard deviation can be smaller than 0.18 m/s for five days and 0.5° × 0.5° grid average.**

***Index Terms*— Doppler Scatterometer (DopScat), maximum likelihood estimation (MLE), measurement accuracy, ocean surface current inversion.**

I. Introduction

OCEAN surface current is driven by wind stress and nonuniform buoyancy forcing caused by differences in atmospheric-ocean fluxes of heat and fresh water. The wind-driven currents and buoyancy differences give rise to the large-scale circulation of the ocean and its associated mass transport [1]. The mesoscale activity of ocean current represents over 98% of the ocean's kinetic energy content and has direct implications for the mixing of water masses and the transport of water properties. The term mesoscale usually refers to oceanic features between 50 and 200 km, which propagate slowly and can persist for several days to several months [2]. Table I lists the characteristic velocities, temporal, and spatial scales of some typical oceanic phenomena [3]. The measurement retrieval accuracy is also highly important. Typically, this must be less than approximately 0.1 m/s during the temporal scale and independent of current regimes.

TABLE I
CHARACTERISTIC VELOCITIES OF SOME TYPICAL OCEANIC PHENOMENA

Phenomenon	Temporal Scale (hr)	Spatial Scale (km)	Velocity Scale (cm/s)
Equatorial Current	240	50-100	10-150
Western Boundary Currents	48	10-100	10-200+
Ocean Mesoscale Eddies	120	10-20	10-50
Ocean Fronts	120	1-5	30

At present, the global ocean current is usually measured by the spaceborne altimeter and synthetic aperture radar (SAR). The geostrophic current can be retrieved from the precise altitude difference of sea surface measured by spaceborne altimeter [4]. But altimeter can only offer the macroscale circulation of ocean surface. Doppler centroid anomaly analysis and along-track interferometry technique can be used in SAR for ocean current measurements [5], [6]. However, SAR is limited by the amount of data, transmit power, swath, etc. Thus, it cannot achieve a global coverage in a high temporal resolution.

Doppler Scatterometer (DopScat) is a new type of radar for ocean remote sensing, which can measure the Doppler frequency shift and echo power simultaneously [7]–[10]. The ocean surface current field (speed and direction) can be retrieved from Doppler frequency shift of radar echoes caused by the motion of sea surface. Meanwhile the ocean surface wind field can be retrieved from the normalized radar cross section (NRCS) of sea surface. The DopScat is based on real aperture radar, which can achieve a very wide swath. It can provide the ocean surface current and wind vector information in a certain resolution and achieve global coverage quickly. It is very important for the marine environment forecasting and climate changes research.

Manuscript received February 20, 2017; revised May 9, 2017 and July 5, 2017; accepted July 9, 2017. Date of publication August 11, 2017; date of current version October 25, 2017. This work was supported in part by the National Research and Development Plan under Grant 2016YFC1401002, in part by the Natural Science Foundation of China under Grant 41606202, and in part by the open fund of Key Laboratory of Space Ocean Remote Sensing and Application under Grant SOA: 201601001. *(Corresponding author: Qingliu Bao.)*

Q. Bao is with the Key Laboratory of Space Ocean Remote Sensing and Application, SOA, National Satellite Ocean Application Service, Beijing 100081, China, and also with the Ministry of Education Key Laboratory for Earth System Modeling, Department of Earth System Science, Tsinghua University, Beijing 100084, China (e-mail: baoqingliu2000@163.com).

M. Lin, Y. Zhang, and S. Lang are with the National Satellite Ocean Application Service, State Oceanic Administration, Beijing 100081, China (e-mail: mslin@mail.nsoas.org.cn; zhangyouguang@mail.nsoas.org.cn).

X. Dong is with the Key Laboratory of Microwave Remote Sensing, National Space Science Center, Chinese Academy of Sciences, Beijing 100190, China.

P. Gong is with the Ministry of Education Key Laboratory for Earth System Modeling, Department of Earth System Science, Tsinghua University, Beijing 100084, China.

Color versions of one or more of the figures in this paper are available online at http://ieeexplore.ieee.org.

Digital Object Identifier 10.1109/TGRS.2017.2728824

0196-2892 © 2017 IEEE. Personal use is permitted, but republication/redistribution requires IEEE permission.
See http://www.ieee.org/publications_standards/publications/rights/index.html for more information.

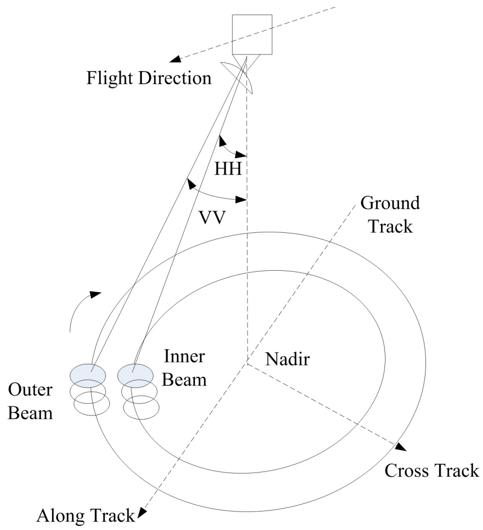

Fig. 1. Observation geometry of DopScat.

It is important to note that spaceborne scatterometers send microwave pulses to the ocean surface and measure the backscatter power. It is modified by surface capillary waves, which are believed to be in equilibrium with the wind stress at the ocean surface. This is converted to a wind speed assuming that the boundary layer over the ocean is neutrally stable. The equivalent neutral winds are uniquely related to the DopScat measurements.

The data processing of DopScat is different from that of traditional scatterometers. The operational wind field inversion method for scatterometer is maximum likelihood estimation (MLE) [11], [12], which is widely used in HY-2A Scat, QuikScat, ASCAT, and so on. The scatterometer retrieval method based on Bayesian inference of posterior maximum likelihood has a better performance [13], [14]. DopScat can obtain the Doppler frequency shift of sea surface apart from NRCS. How to use this information to retrieve the ocean surface current is the main topic of this paper. The measurement principle of DopScat is introduced briefly in Section II. The ocean surface current inversion method for DopScat is described in Section III. Section IV gives the simulation model of DopScat. Section V shows the ocean surface current inversion results and analyzes the retrieval accuracy. The global ocean surface current measurement is analyzed in Section VI. At last, the conclusion is drawn in Section VII.

II. Measurement Principle of DopScat Based on Pencil Beam

A. Observation Geometry

This DopScat takes pencil-beam rotating as its observation geometry, which is similar as that of QuikScat [15], [16] and HY-2A Scat [17]. The observation geometry of DopScat is shown in Fig. 1. The inner beam is HH polarization and the outer beam is VV polarization. The observation geometry parameters of DopScat are listed in Table II.

TABLE II
Observation Geometry Parameters of DopScat

Orbit Parameters	
orbit height	963 km
orbit inclination	98.616°
eccentricity ratio	0
satellite velocity	7373 m/s
Geometry Parameters	
polarization	HH(inner)/VV(outer)
local incident angle	41°/48°
swath	1400 km/1800 km
footprint in cross track	22.6 km/28.5 km
footprint in along track	17 km/18.9 km

B. Measurement Principle

DopScat on based on pencil-beam rotating observation geometry measures the Doppler frequency shift of radar echoes by interpulse interference, which is proposed in [18]. When t is zero, the distance between the radar and the target is $r(t = 0)$. When t equals τ, the distance between the radar and the target is $r(t = \tau)$. The distance difference of the target at these two moments is Δr and the phase difference of the radar echoes at these two moments is $\Delta\phi$. The relationship between $\Delta\phi$ and Δr can be expressed as

$$\Delta\phi = 2k\Delta r \tag{1}$$

where k is the wavenumber of radar electromagnetic wave. The radial velocity component can be written as

$$V_r = \frac{\Delta r}{\tau} = \frac{\Delta\phi}{2k\tau}. \tag{2}$$

By radial velocity components V_{r1} and V_{r2} that were observed at two different azimuth angles, we can estimate the velocity vector of the target. The interferometry schematic of DopScat is shown in Fig. 2(a), and the schematic of velocity vector resultant is shown in Fig. 2(b) [18].

III. Ocean Surface Current Inversion Method

Several optimization techniques, which depend on the desired statistical objective, can be applied when using the Bayesian approach, including maximum likelihood, maximum posterior probability, minimum variance, minimum measurement error, etc. The MLE is the most commonly used technique to invert winds in scatterometry [11].

For the ocean surface current inversion of DopScat, we can also use the MLE technique. Different from the wind speed inversion of traditional scatterometer, DopScat can obtain the NRCS and Doppler frequency shift of sea surface simultaneously. We need to establish the MLE that is suitable for ocean surface current of DopScat.

A. Objective Function

The objective function represents the probability of a trial wind/current vector (solution) being the true wind/current. The objective function can be interpreted as the distance between measurement values and the solution set lying on

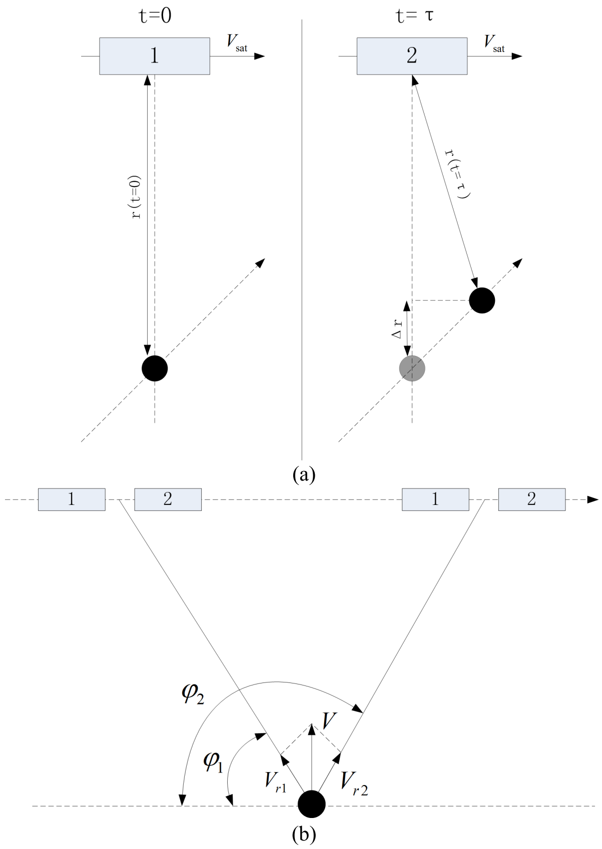

Fig. 2. Measurement principle schematic of DopScat. (a) Interferometry schematic. (b) Velocity vector resultant.

the geophysical model function (GMF) surface [19]. The shape of the MLE objective function is mainly determined by the GMF surface modulated by azimuth and the relative geometry among views [20]. By using the MLE objective function minima in the retrieval, the maximum probability solution can be obtained in some relatively ideal conditions. The shape of the objective function will determine the skill of the wind/current retrieval. For SeaWinds, the standard MLE objective function is defined as [14]

$$\mathrm{MLE} = \frac{1}{N}\sum_{i=1}^{N}\frac{\left(\sigma^0_{\mathrm{mi}} - \sigma^0_{\mathrm{si}}\right)^2}{kp\left(\sigma^0_{\mathrm{si}}\right)} \tag{3}$$

where N is the number of measurements, σ^0_{mi} is the backscatter measurement, σ^0_{si} is the backscatter simulated through the GMF for different wind speeds and direction trial values, and $kp(\sigma^0_{\mathrm{si}})$ is the measurement error variance.

For DopScat, we can obtain the sea surface Doppler frequency shift apart from the NRCS. The Doppler frequency shift is unambiguous with wind direction. The Doppler frequency shift will be very useful for the wind direction inversion. In order to retrieve the ocean surface current, the MLE objective function, as (3), need to be modified. Thus, we established the MLE objective that is suitable for DopScat to retrieve the ocean surface current and wind field simultaneously.

Assuming that a current vector cell has N-NRCS and M-Doppler frequency shift measurements in approximately the same time and location. During the measurements, probably dozens of seconds to several minutes, the neutral stability wind field vector (U_{wind}, ϕ_{wind}) at 10 m height and ocean surface current field vector (U_{current}, ϕ_{current}) are assumed as unchanged. If it is assumed that the errors of each measurement are independent, the joint probability density function of measurement errors can be expressed as [21]

$$\begin{aligned} p\left(R^\sigma_1, \ldots, R^\sigma_N, R^f_1, \ldots, R^f_M \mid (U_{\mathrm{wind}}, \phi_{\mathrm{wind}}, U_{\mathrm{current}}, \phi_{\mathrm{current}})\right) \\ = \prod_{i=1}^{N} p\left(R^\sigma_i \mid (U_{\mathrm{wind}}, \phi_{\mathrm{wind}})\right) \\ \cdot \prod_{i=1}^{M} p\left(R^f_i \mid (U_{\mathrm{wind}}, \phi_{\mathrm{wind}}, U_{\mathrm{current}}, \phi_{\mathrm{current}})\right) \end{aligned} \tag{4}$$

where R^σ_i is the residual error of NRCS measurement, and R^f_i is the residual error of Doppler frequency shift measurement. R^σ_i and R^f_i are the normally distributed variable with zero mean [21]. The variance of R^σ_i can be expressed as $V_{R^\sigma_i}$, and the variance of R^f_i can be expressed as $V_{R^f_i}$. Taking the logarithm on both sides of (4), we can obtain the MLE objective function of DopScat, shown as (5), as shown at the bottom of the page, where σ_i is the measured NRCS, and f_i is the measured Doppler frequency shift. M_{Sigma} is the empirical backscattering GMF model. For the Ku-band scatterometer, we use the NSCAT-2 as the empirical backscattering GMF model. M_{Doppler} is the sea surface Doppler spectrum model, which will be introduced in the next section. V_{R^σ} is the variance of backscatter measurement errors which can be expressed as [22]

$$V_{R^\sigma} = K_p^2 \cdot \sigma_0^2. \tag{6}$$

The detail of Kp is introduced in Section IV. V_{R^f} is the variance of Doppler frequency shift measurement errors which can be written as

$$V_{R^f} = S^2_{\mathrm{fc}} + S^2_{\mathrm{fr}} + S^2_{\mathrm{fm}} \tag{7}$$

$$\begin{aligned} J_{\mathrm{MLE}}(U_{\mathrm{wind}}, \phi_{\mathrm{wind}}, U_{\mathrm{current}}, \phi_{\mathrm{current}}) = -\sum_{i=1}^{N}\left[\frac{(\sigma_i - M_{\mathrm{Sigma}}(U_{\mathrm{wind}}, \phi_{\mathrm{wind}} - \phi_i, \theta_i, p_i))^2}{2V_{R^\sigma_i}} + \ln\sqrt{V_{R^\sigma_i}}\right] \\ -\sum_{j=1}^{M}\left[\frac{(f_j - M_{\mathrm{Doppler}}(U_{\mathrm{wind}}, \phi_{\mathrm{wind}} - \phi_j, U_{\mathrm{current}}, \phi_{\mathrm{current}} - \phi_j, \theta_j, p_j))^2}{2V_{R^f_j}} + \ln\sqrt{V_{R^f_j}}\right] \end{aligned} \tag{5}$$

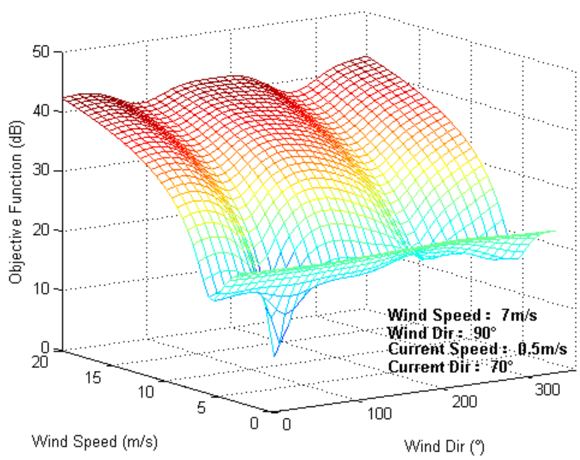

Fig. 3. Characters of objective function.

where S_{fc} is the Doppler frequency measurement error which is determined by signal-to-noise ratio (SNR), pulse repetition frequency (PRF), and antenna size. S_{fr} is the Doppler frequency calibration error which is related to satellite attitude and velocity measurement errors. S_{fm} is the model error which is determined by the accuracy of Doppler frequency GMF model.

The wind and current field inversion is searching a suitable wind and current vector to make (5) reaches its maximum. Due to NRCS has a double harmonic dependence on vector winds, while Doppler frequency shift is a single harmonic. Thus, the Doppler frequency shift is unambiguous with wind direction. Equation (5) does not have ambiguous solutions normally. The global maximum of the objective function will be the MLE solution of wind and current vectors. We do not need extra wind direction information to remove the ambiguous solutions. The characters of objective function with different wind speeds and wind directions are shown in Fig. 3. The objective function shown in Fig. 3 is negative of (5).

B. Sea Surface Doppler Spectrum Model

Sea surface Doppler spectrum is a very important model in ocean surface current inversion, shown as M_{Doppler} in (5). The error of sea surface Doppler spectrum model is related to inversion accuracy directly. In 2000, Romeiser and Thompson [23] established a numerical Doppler spectrum model for along-track interferometric radar ocean surface current measurement. Fois *et al.* [24] established an analytical model for the description of the full-polarimetric sea surface Doppler signature in 2015. In this paper, we use the numerical Doppler spectrum established by Romeiser to calculate the Doppler spectrum in Ku-band. It is based on Bragg scattering theory in a composite surface model approach. The input parameters of Doppler spectrum model, including ocean wave spectrum and directional distribution functions, affect the Doppler spectrum computation severely. Thus, an empirical GMF in C-band (CDOP) is compared with the numerical calculation results to select the most suitable input parameters.

The CDOP model is derived from the Doppler centroid anomaly of ENVISAT ASAR. It is used to predict Doppler

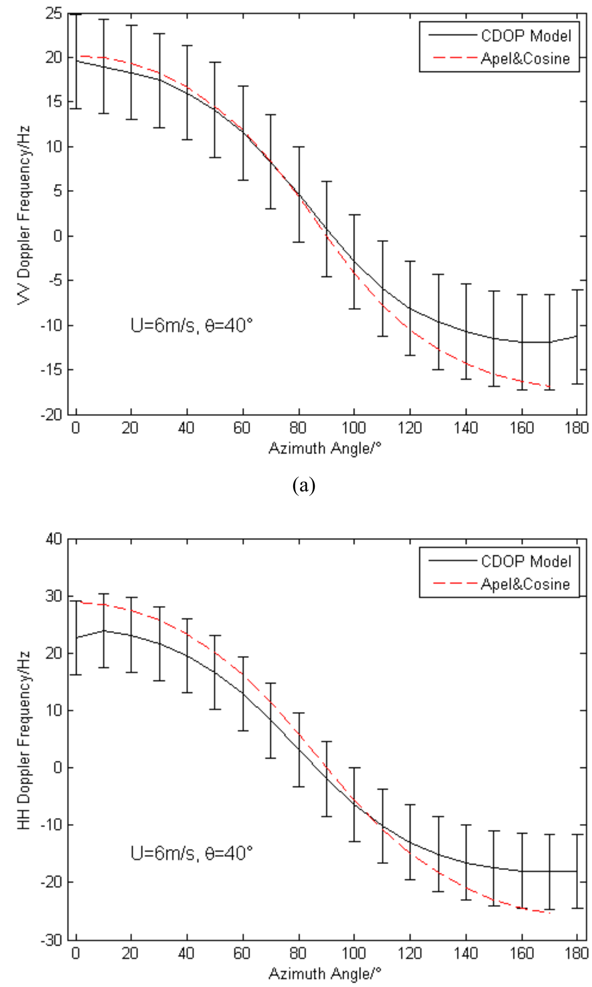

(a)

(b)

Fig. 4. Comparison of simulated Doppler frequency shift with CDOP model. (a) VV polarization. (b) HH polarization.

shifts at both VV and HH polarizations as a function of wind speed, radar incidence angle, and wind direction with respect to radar look direction. Thus, the CDOP model can be expressed as [25], [26]

$$f_D = \mathrm{CDOP}(\phi, u_{10}, \theta, \mathrm{pol}) \tag{8}$$

where f_D represents the Doppler frequency anomaly, ϕ is the wind direction with respect to radar look direction, u_{10} is the wind speed at 10 m height, θ is the incident angle, and pol is for VV or HH.

By the input parameters selection, we choose cosine-shape directional distribution function [27] and Apel spectrum [28] as the inputs in the numerical Doppler spectrum calculation. Then, the Doppler frequency shift versus azimuth angle for both VV and HH polarizations in C-band is simulated and compared with the CDOP model. The wind speed is 6 m/s and the incident angle is 40°. The comparison of simulated Doppler frequency shift with CDOP model is shown in Fig. 4. The CDOP model is plotted in the method of error bar.

From Fig. 4, we can see that simulated Doppler frequency shift is basically consistent with the CDOP model. At upwind and downwind directions the simulated Doppler frequency shift is little bigger than the CDOP model, but still within

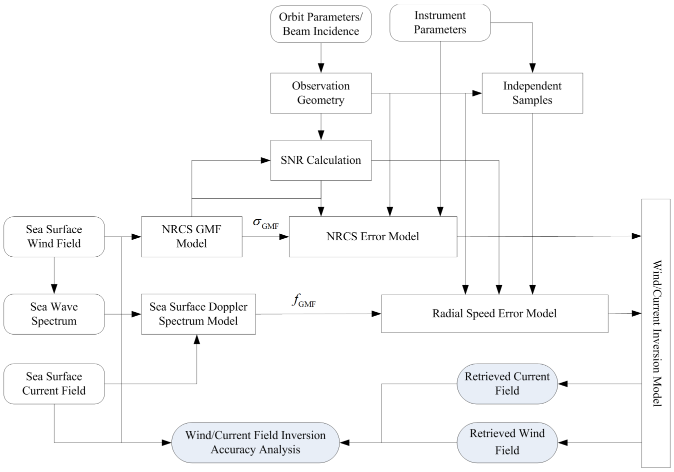

Fig. 5. Simulation flow of DopScat system.

the root mean square of CDOP model. For HH polarization, the Doppler frequency shift differences in upwind and downwind directions are smaller than 7 Hz.

The Doppler frequency shift at Ku-band is about twice larger than that at C-band. Thus, the Doppler frequency error at Ku-band is also nearly twice larger than that at C-band. But the ocean surface Doppler spectrum has no significant effect on the ocean current inversion, because we use the same Doppler spectrum in the forward and inversion simulation models.

IV. Simulation Model

A. Simulation Flow

In this section, we established an "end-to-end" simulation model to analyze the measurement and inversion accuracy of DopScat. The input parameters of the simulation model include sea surface wind field, sea surface current field, instrument parameters, and orbit parameters. And the output parameters include the retrieved wind field vector, retrieved current field vector, and their inversion accuracy. The simulation flow of DopScat system is shown in Fig. 5.

The kernel of the DopScat simulation model is the radial velocity error model, backscattering coefficient error model, and wind/current field inversion model which is introduced in Section III. There are two GMF models used in the DopScat simulation: the backscattering GMF model and the Doppler frequency shift GMF, which are the bridges between oceanography parameters to radar measurement parameters. In our simulation, we use the NSCAT-2 empirical model as the backscattering GMF and the numerical sea surface Doppler spectrum model suggested by Romeiser as the Doppler frequency shift model which is introduced in Section III-B.

The outputs of DopScat simulation model are the wind/current field vector and the inversion accuracy. The wind/current field inversion accuracy is evaluated by two index: bias and standard deviation (Std), which are defined as

$$\mathrm{Bias} = \frac{1}{N}\sum_{\mathrm{i}=1}^{N}(U_{\mathrm{ri}} - U_{\mathrm{ti}}) \tag{9}$$

$$\mathrm{Std} = \sqrt{\frac{1}{N}\sum_{i=1}^{N}(U_{\mathrm{ri}} - U_{\mathrm{ti}} - \mathrm{Bias})^2} \tag{10}$$

TABLE III
Main Parameters of DopScat

Antenna Parameters	
beam width in azimuth(dimension)	0.8°(1.8m)
beam width in range(dimension)	0.8°(1.8m)
antenna incident angle	35°(HH)/41°(VV)
antenna gain	48 dB
rotation rate	18 rpm
scan loss	3 dB
Signal Parameters	
carrier frequency	13.5 GHz
transmitted power	500 W
PRF	12 kHz
bandwidth	5 MHz
system loss	5 dB
system temperature	300K

where U_{ri} is the retrieved wind speed, wind direction, current speed, or current direction; U_{ti} is the true wind speed, wind direction, current speed, or current direction; N is the number of samples.

B. System Parameters

This DopScat is a pencil-beam rotating radar and measures the target in both VV and HH polarizations. In order to measure the Doppler frequency shift, the radar system parameters should be optimized, especially the antenna dimension, PRF, and bandwidth [9], [10].

Antenna dimension determines the antenna gain and Doppler bandwidth. The larger the antenna dimension, the better the radar performance. While, oversize of antenna will increase the engineering difficulty. Thus, the antenna dimension must satisfy its engineering feasibility.

PRF determines the maximum pulselength and duty cycle, which are directly related to the SNR. The higher PRF, the smaller spatial decorrelation. A trade-off exists, however, because as PRF increase, SNR decrease, and the thermal decorrelation is larger.

If we use a larger bandwidth, we will get higher resolution in range direction, and then there will be more independent samples. However, noise power will increase and SNR will decrease with larger bandwidth. Thus, a trade-off also exists between bandwidth and SNR.

In our simulation, the orbit and observation geometry parameters of DopScat are successive from the HY-2A scatterometer which is listed in Table II. The main DopScat parameters in the simulation are shown in Table III.

C. Backscattering Coefficient Error Model

The measurement accuracy of σ_0 is the main factor that should be considered in the scatterometer design. Normally, the measurement error of σ_0 is normalized in the form of standard deviation (Kp)

$$K_p = \frac{\sqrt{\mathrm{var}\left[\sigma_0\right]}}{\varepsilon[\sigma_0]} \tag{11}$$

where var[·] represents the mean variance of one physical quantity and $\varepsilon[\cdot]$ represents its mean value. The contribution of Kp is mainly from the measurement error of radar echoes, the calibration factor error, and geophysical noise. The former is usually named communication error (Kpc). It is caused by the signal fading which is the intrinsic character of radar systems and receiver thermal noise. It is a function of SNR and independent samples. The calibration factor error is usually named as calibration error (Kpr). It is caused by the uncertainty of radar parameters, such as antenna gain and system loss. What is more, the GMF is slightly different from the true value. The model error (Kpm) is caused by GMF model in the process of inversion and σ_0 calibration using the ground area target and its backscattering coefficient model. Generally, the communication error (Kpc), calibration error (Kpr), and model error (Kpm) are independent and Gaussian distributed with zero mean. Thus, the Kp can be expressed as [29]

$$K_p = \sqrt{K_{\text{pc}}^2 + K_{\text{pr}}^2 + K_{\text{pm}}^2}. \tag{12}$$

D. Radial Velocity Error Model

The radial velocity error model of DopScat consists three parts: radial velocity measurement error, platform velocity estimate error, and Doppler spectrum model error. These three parts are assumed as Gaussian distributed and independent to each other. Thus, the radial velocity error can be expressed as

$$\Delta V_{\text{radial}} = \sqrt{\Delta V_{\text{measure}}^2 + \Delta V_{\text{platform}}^2 + \Delta V_{\text{model}}^2} \tag{13}$$

where ΔV_{radial} is the radial velocity error, $\Delta V_{\text{measure}}$ is the radial velocity measurement error which is related to the radar system parameters and observation geometry, $\Delta V_{\text{platform}}$ is the platform velocity estimate error which is mainly determined by the satellite attitude measurement error, and ΔV_{model} represents the Doppler spectrum model error.

1) Radial Velocity Measurement Error: Radial velocity measurement error $\Delta V_{\text{measure}}$ is determined by interferometric phase measurement error σ_ϕ directly. The relationship between radial velocity measurement error and interferometric phase measurement error can be written as

$$\Delta V_{\text{measure}} = \frac{\lambda}{4\pi\tau}\sigma_\phi \tag{14}$$

where λ is the radar electromagnetic wavelength and τ is the time interval of pulse echo. Usually, the interferometric phase can be estimated and the estimation error is determined by the correlation coefficient. The correlation coefficient γ can be expressed as the product of four items [9], [30]

$$\gamma = \gamma_{\text{thermal}} \cdot \gamma_{\text{footprint}} \cdot \gamma_{\text{spatial}} \cdot \gamma_{\text{temporal}} \tag{15}$$

where γ_{thermal} is the thermal noise decorrelation, $\gamma_{\text{footprint}}$ is the mismatch decorrelation, γ_{spatial} is the spatial decorrelation, and γ_{temporal} is the temporal decorrelation. The definition and expression of these four decorrelations can be seen in [9] and [30].

By the calculation and analysis, we find that the correlation coefficient γ is mainly determined by the thermal noise decorrelation γ_{thermal} and spatial decorrelation γ_{spatial}. For spaceborne scatterometer, the SNR is usually very low. Thus, the thermal noise decorrelation will be the main decorrelation factor, especially in the low wind speed condition. At the far edge of the swath, the Doppler bandwidth is large. That is where the spatial decorrelation will be the main decorrelation factor. In the simulation model, the radial velocity measurement error at different positions of the swath and of different wind speeds is shown in Fig. 6.

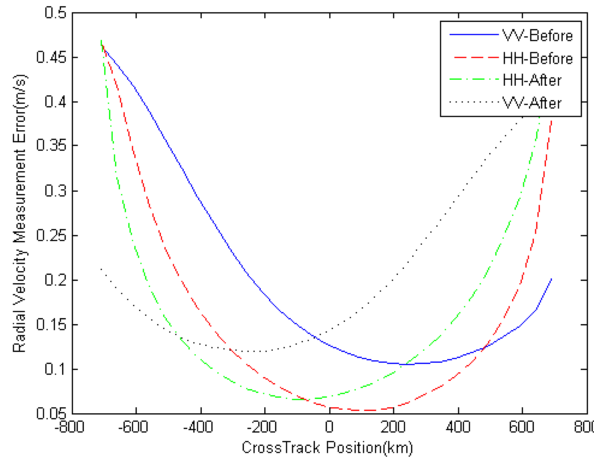

(a)

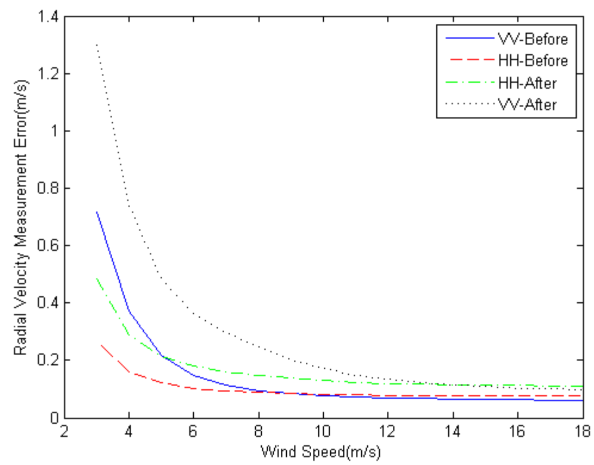

(b)

Fig. 6. Radial velocity measurement error. (a) Different positions of the swath. (Wind speed is 7 m/s.) (b) Different wind speeds. (The position of swath is 400 km).

2) Platform Velocity Estimate Error: The platform velocity estimate error is mainly determined by two factors: satellite speed measurement error and satellite attitude measurement errors [30], where the satellite attitude include the yaw, pitch, and roll. The platform velocity estimation error caused by satellite speed measurement error is negligible. When the satellite velocity measurement error is smaller than 0.02 m/s, the platform velocity estimate error will be smaller than 1 cm/s. The platform velocity estimate error caused by pitch and yaw measurement error is much larger than that of roll, especially in the cross-track direction. The platform velocity estimate error with attitude measurement error for different azimuth angles is shown in Fig. 7.

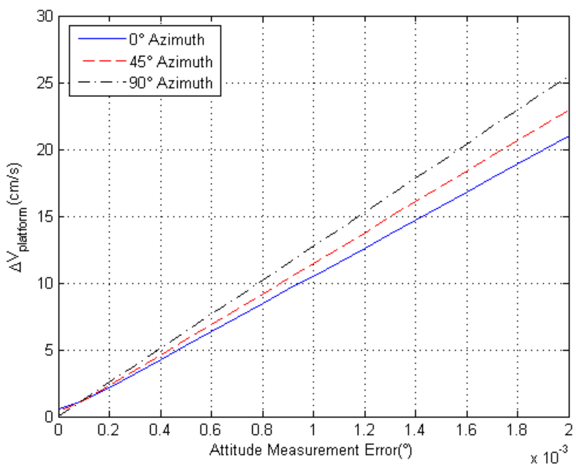

Fig. 7. Platform velocity estimate error with attitude measurement error.

From Fig. 7, we can see that the platform velocity estimate error increases with attitude measurement error linearly. As the development of attitude control and measurement technique, the satellite attitude measurement accuracy can achieve very high accuracy. After the processing of precise orbit and attitude determination, the satellite attitude measurement accuracy can be better than 0.001°, and the satellite speed measurement error can be smaller than 0.3 cm/s.

3) Doppler Spectrum Model Error: The MLE inversion method is used to retrieve the ocean surface current, which is introduced in Section III. The sea surface Doppler spectrum is a very important model in the MLE inversion method, which determines the ocean surface current retrieval accuracy directly. The relationship between Doppler frequency shift error and radial velocity error can be expressed as

$$\Delta V_{\text{model}} = \frac{\Delta f_{\text{model}} \cdot \lambda}{2} \tag{16}$$

where Δf_{model} is the Doppler frequency shift model error, ΔV_{model} is the radial velocity error, and λ is the electromagnetic wavelength.

By the comparison of numerical Doppler spectrum model with the CDOP model (see Section III-B), the Doppler frequency shift error is smaller than 7 Hz in up/down wind direction for HH polarization, where their inconsistency is biggest. Thus, we set the radial velocity error caused by Doppler spectrum model to be 0.1 m/s in the DopScat simulation.

V. Ocean Surface Current Inversion Accuracy Analysis

In this section, we adopt the MLE to retrieve the ocean surface current and Monte Carlo method to analyze its inversion accuracy. The retrieval results are compared with the inputs of DopScat simulation model. The current inversion performance of DopScat for different cross-track positions, wind speed, and current speed are shown as below.

A. Different Cross-Track Positions

For the DopScat, different cross-track positions correspond to different Doppler bandwidths. At the far edge of the swath, Doppler bandwidth is large and the spatial decorrelation is serious. Thus, the correlation coefficient is low and the radial velocity measurement error is large. Meanwhile the radial velocity error determined the ocean current retrieval accuracy directly. The MLE method is used for the ocean surface current inversion. In this section, we simulated the ocean surface current inversion accuracy for medium wind speed condition. The wind speed is 7 m/s, the current speed is 0.5 m/s, and the current cell is 50 km × 50 km. The current speed component inversion accuracy in cross-track and along-track directions is shown in Fig. 8.

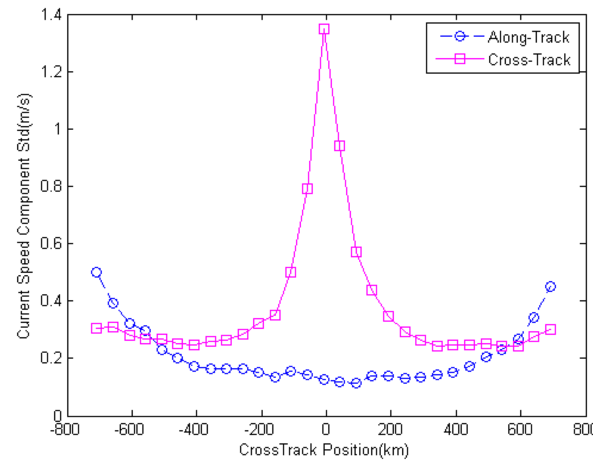

Fig. 8. Current speed component inversion accuracy for different cross-track positions.

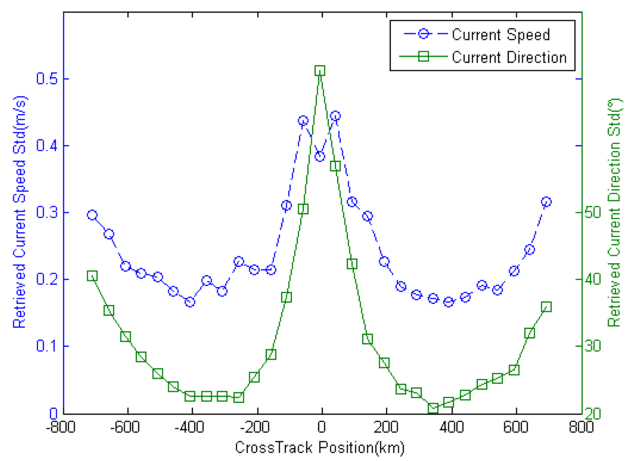

Fig. 9. Current speed and direction inversion accuracy for different cross-track positions.

From Fig. 8, we can see that the inversion error of current speed component in both along-track and cross-track directions is smaller than 0.35 m/s basically. But for cross-track direction, the current speed inversion error is much larger nearby the nadir. That is due to the observation azimuth of DopScat at nadir is opposite, thus the radial velocity observed at nadir lack the component in cross-track direction.

The statistical analysis of the retrieved current speed and direction accuracy is shown in Fig. 9. At the far edge of swath and nadir, the current speed and direction inversion

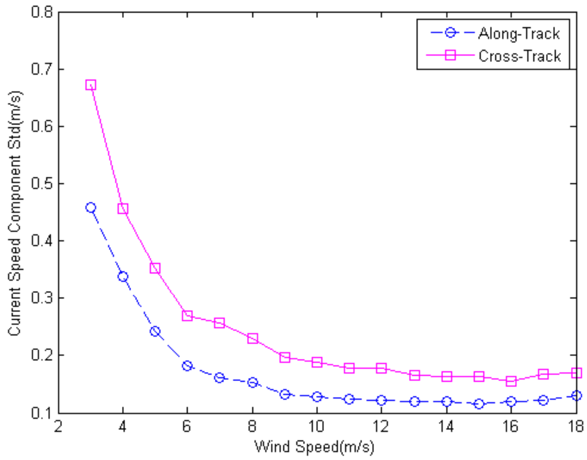

Fig. 10. Current speed component inversion accuracy for different wind speeds.

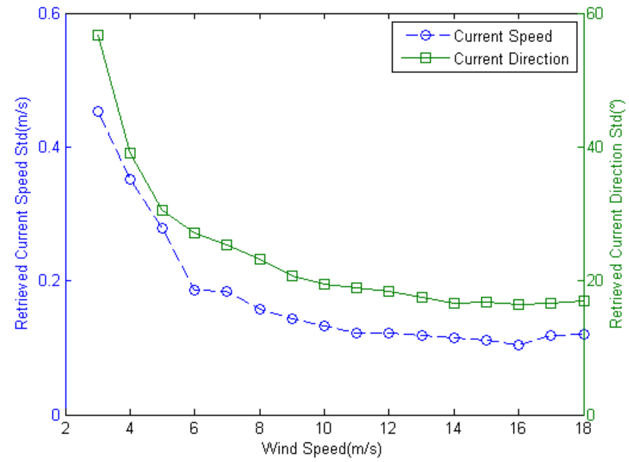

Fig. 11. Current speed and direction inversion accuracy for different wind speeds.

accuracy are poor. And at the middle of swath on each side, the performance of DopScat on current field measurement is best. For most cross-track position, the current speed retrieval accuracy is better than 0.3 m/s and the current direction retrieval accuracy is better than 30°.

B. Different Wind Speeds

Sea surface wind speed is a very important parameter that affects the DopScat on ocean current field measurement. Wind speed determines the sea surface NRCS and then the radar SNR. Thermal decorrelation, which is related to the SNR, will be the most dominating decorrelation factor in the low wind speed condition. The ocean surface current component retrieval accuracy for different wind speeds is shown in Fig. 10. In the simulation, current speed is set as 0.5 m/s, cross-track position is chosen as 400 km, and the current field cell is set as 50 km × 50 km.

From Fig. 10, we can see that the current speed component inversion accuracy improves, in both along-track and cross-track directions, with the increase of wind speed. When the wind speed is larger than 7 m/s, this trend tends to be gentle. And the current speed component standard deviation is to be 0.2 and 0.13 m/s for cross-track and along-track directions, respectively. The statistic of the retrieved current speed and direction accuracy for different wind speeds is shown in Fig. 11.

The trend of retrieved current speed and direction accuracy with wind speed is similar with that of Fig. 10. When the wind speed is larger than 7 m/s, the current speed retrieval uncertainty can be smaller than 0.18 m/s, and the current direction retrieval accuracy can be better than 25°.

C. Different Current Velocities

The velocity of ocean current field will affect its inversion accuracy as well. Usually, the current speed is smaller than 1.5 m/s for open sea. In this section, we simulated the ocean current speed and direction inversion accuracy for different current velocities. The wind speed is set as 7 m/s and the current field cell is set as 50 km × 50 km in the simulation. The ocean surface current component retrieval accuracy for different current velocities is shown in Fig. 12.

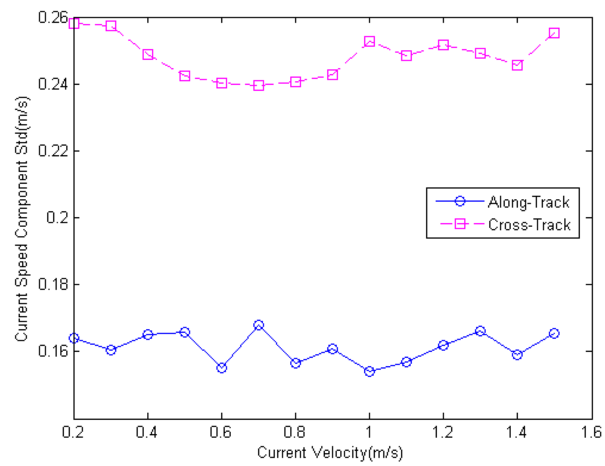

Fig. 12. Ocean surface current component retrieval accuracy for different current velocities.

The current velocity does not affect the current speed component retrieval accuracy basically, as shown in Fig. 12. The ocean surface current component standard deviation is about 0.25 and 0.16 m/s for cross-track and along-track direction. The statistic of the retrieved current speed and direction accuracy for different current velocities is shown in Fig. 13.

From Fig. 13, we can see that the current speed inversion accuracy decreases slightly when the current velocity is smaller than 0.5 m/s. In general, the current speed retrieval standard deviation is smaller than 0.16 m/s and larger than 0.14 m/s. However, the current direction inversion accuracy improves obviously with the increase of current velocity. When the current velocity is larger than 0.6 m/s, the current direction retrieval standard deviation is smaller than 22°.

VI. Global Ocean Surface Current Measurement

A. Input Global Current/Wind Map

In the simulation of DopScat, we use the Ocean Surface Current Analyses Real-time (OSCAR) product as current input. OSCAR is a NASA-funded research project and global

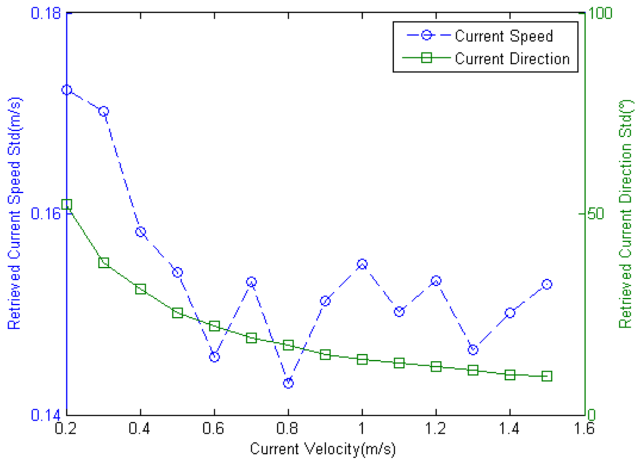

Fig. 13. Statistic of current speed and direction accuracy for different current velocities.

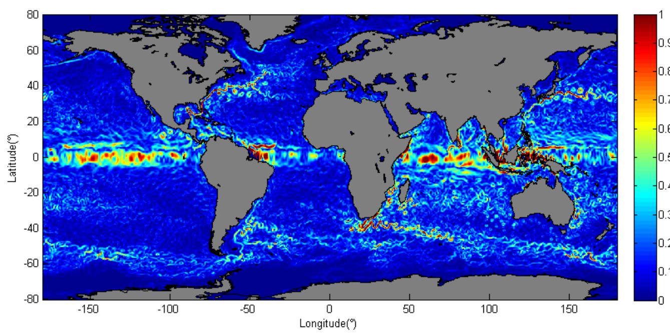

Fig. 14. Global current speed map on January 1, 2015.

surface current database. OSCAR global ocean surface mixed layer velocities are calculated from satellite-sensed sea surface height gradients, ocean vector winds, and sea surface temperature fields using geostrophy, Ekman, and thermal wind dynamics. Surface currents are provided on global grid every five days, dating from 1992 to the present day, with daily updates and near-real-time availability. The NASA PO.DAAC site serves OSCAR currents on both 1° and 1/3° grid spacing in netcdf format. We should note that the model calculates a surface current averaged over the top 30 m of the upper ocean. The global current speed map provides by OSCAR on January 1, 2015 is shown in Fig. 14.

From Fig. 14, we can see that the ocean current speed is small for most of the sea areas. It is smaller than 0.1 m/s generally. In some typical areas, the current speed is larger than 0.5 m/s, such as Equatorial Current, Gulf Stream, Kuroshio, and Agulhas Current.

In the DopScat simulation, we use the European Centre for Medium-Range Weather Forecasts (ECMWF) reanalysis product as its wind input. ECMWF is an independent intergovernmental organization. It is both a research institute and an operational service, producing and disseminating numerical weather predictions to its member states. The time interval of ECMWF forecasting and reanalysis product is 6 h. The 0.5° × 0.5° grid spacing reanalysis wind field product on January 1, 2015 is shown in Fig. 15.

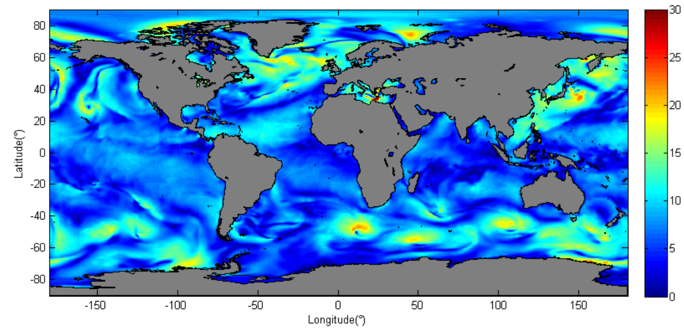

Fig. 15. ECMWF reanalysis wind field on January 1, 2015.

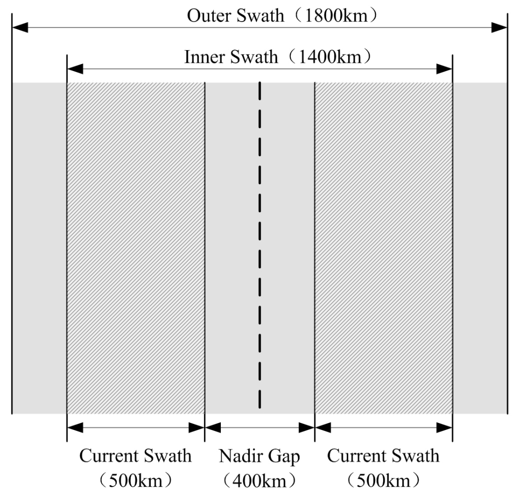

Fig. 16. Diagram of effective swath for ocean current inversion.

B. Retrieved Global Current Map

The swath of DopScat is about 1800 km, as shown in Table II. In the global current field observation, we do not use the measurements near nadir to retrieve the ocean surface current where the current inversion accuracy is poor. The width of swath that has been used to retrieve the ocean current is about 1000 km for 500 km on each side and with a 400-km gap on nadir. The diagram of effective swath for ocean current inversion is shown in Fig. 16. In Fig. 16, the slash shadow shows the swath used for ocean current inversion.

In the global ocean current field observation, the orbit parameters of DopScat is successive from the HY-2A satellite. The main orbit and system parameters of DopScat are listed in Table II. The ocean current inversion method is MLE that introduced in Section III. The global ocean current observation results for 0.5° × 0.5° grid spacing is shown in Fig. 17.

From Fig. 17, we can see that after days average the ocean current measurement accuracy has further improved. The typical areas where the current speeds are strong, such as Equatorial Current, Gulf Stream, Kuroshio, and Agulhas Current, are distinct. Some mesoscale eddies are apparent. But the retrieved ocean current is slight biased, especially in the weak current area. The quantitative analysis of the global ocean current speed retrieval accuracy is listed in Table IV.

As shown in Table IV, the retrieved global current speed standard deviation can be smaller than 0.18 m/s with a bias of about 0.1 m/s for five days and 0.5° × 0.5° grid average.

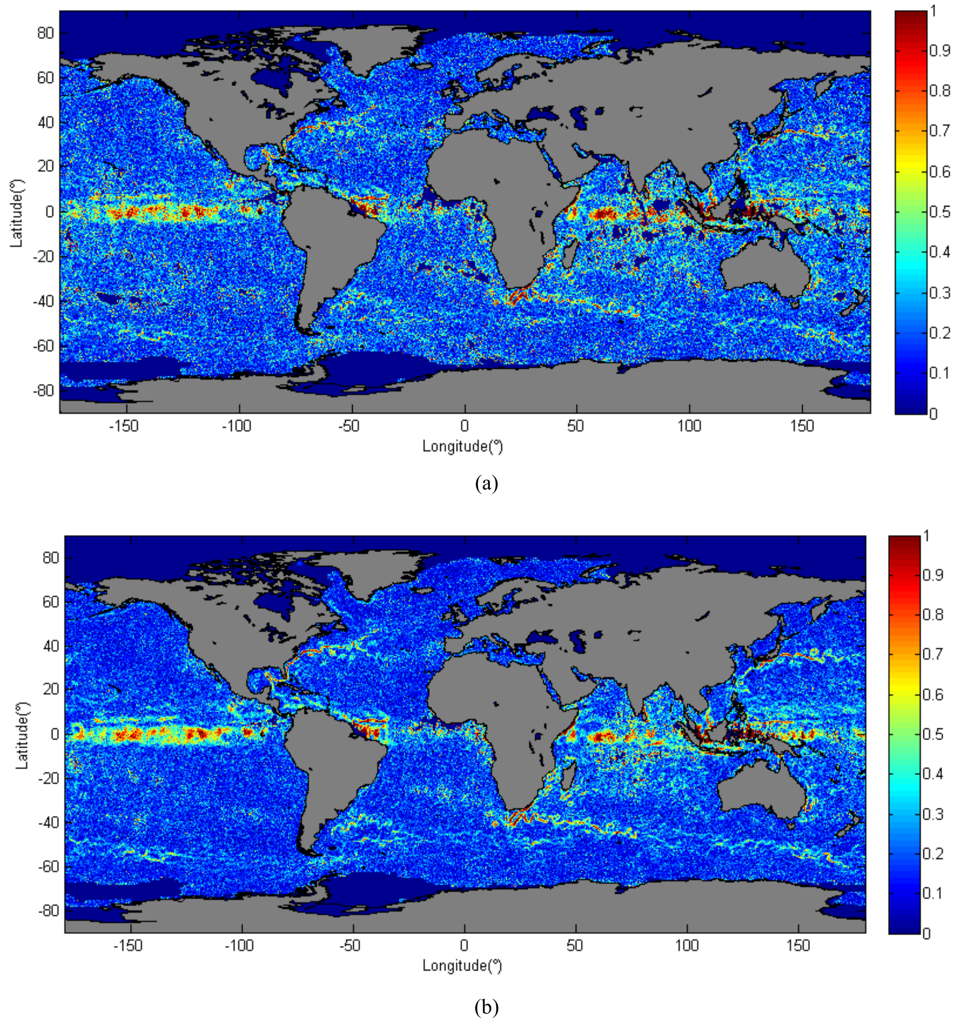

Fig. 17. Global ocean current observation results for $0.5° \times 0.5°$ grid spacing. (a) Five days average (b) Ten days average.

TABLE IV
RETRIEVAL ACCURACY OF GLOBAL OCEAN CURRENT SPEED

Temporal/Spatial resolution		Current Speed Std	Current Speed Bias	Correlation Coefficient
5 days	0.5°×0.5°	0.1797 m/s	0.1018 m/s	0.5101
	1.0°×1.0°	0.1298 m/s	0.0240 m/s	0.6554
10 days	0.5°×0.5°	0.1325 m/s	0.0551 m/s	0.6667
	1.0°×1.0°	0.1099 m/s	-0.0002 m/s	0.7434

The correlation coefficient of global current speed map is larger than 0.5. The current speed standard deviation and bias will decrease with the increase of temporal and spatial resolution. However, long time and large space average will filter the quick-changing information of the ocean current. The temporal and spatial resolution of the global ocean surface current product should be selected according to the application requirement.

The statistical current direction inversion accuracy in global current map retrieval is shown in Fig. 18. The results are for five days and $0.5° \times 0.5°$ grid average.

From Fig. 18, we can see that retrieved current direction standard deviation decrease with the current speed, which is similar with that of Fig. 13. When the current speed is larger than 0.5 m/s, this improvement is to be gentle and the retrieved current direction standard deviation is smaller than 26°.

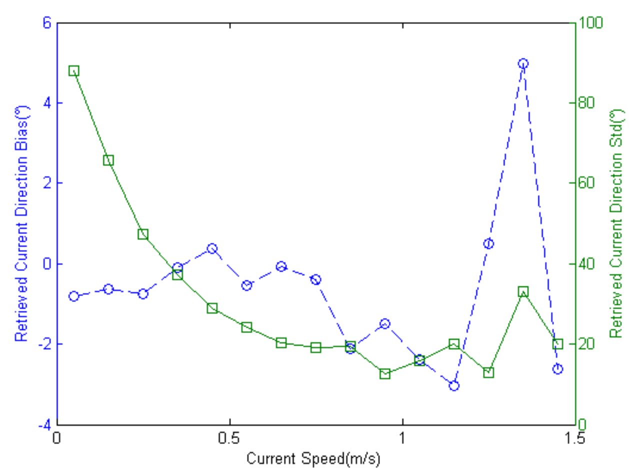

Fig. 18. Statistical current direction inversion accuracy with current speed for five days and $0.5° \times 0.5°$ grid average.

VII. CONCLUSION

Ocean surface current is driven by wind stress and nonuniform buoyancy forcing caused by differences in atmospheric-ocean fluxes of heat and fresh water. It is one of the very important ocean dynamic parameters, which have been widely used in industry and research. DopScat is a new type of radar for ocean remote sensing, which can measure the Doppler frequency shift and echo power simultaneously. The ocean surface current field (speed and direction) can be retrieved from the Doppler frequency shift of radar echoes caused by the motion of sea surface. Meanwhile the ocean surface wind field can be retrieved from the NRCS of sea surface.

In this paper, we establish the ocean surface current inversion method for DopScat. The objective function of the MLE is given in Section III. Meanwhile, we use the empirical GMF in C-band (CDOP) to select the most suitable input parameters of ocean Doppler spectrum model in Ku-band.

In order to analysis the ocean current inversion accuracy, we establish the simulation model of DopScat. The backscattering coefficient error model and radial velocity error model are the heart of the DopScat simulation. The ocean current inversion accuracy is analyzed by the Monte Carlo method. The simulation results show that the inversion error of current speed component in both along-track and cross-track directions is smaller than 0.35 m/s, respectively, for single measurement in medium wind speed condition.

At last, we simulate the global ocean current measurement using the DopScat simulation model and the MLE inversion method that introduced in Sections III and IV. From the simulation results, we can see that the typical ocean current areas are distinct, such as Equatorial Current, Gulf Stream, Kuroshio, and Agulhas Current. The retrieved global current speed standard deviation can be smaller than 0.18 m/s with a bias of about 0.1 m/s for five days and $0.5^\circ \times 0.5^\circ$ grid average.

What is more, we also analyzed the ocean surface wind retrieval accuracy of DopScat based on pencil-beam rotating observation geometry. The standard deviation of retrieved wind speed is smaller than 1 m/s basically. It is better than that of the existing HY-2A scatterometer. That is mainly due to the system parameters of DopScat is more advanced than the existing HY-2A scatterometer. For example, the antenna gain and the transmit power of DopScat is higher than the existing HY-2A scatterometer. However, at very low wind speed, the wind direction retrieval performance is poor. The standard deviation of retrieved wind direction will be larger than 20° when the wind speed is smaller than 5 m/s. For low wind speed, the radar echo SNR is small and the Doppler frequency shift estimation error is large. Meanwhile, the radial velocity cause by wind blowing is small. Thus, the retrieved wind is usually blowing in an opposite direction. In the future, we need do much more work to improve the wind direction retrieval performance for low wind speed condition.

ACKNOWLEDGMENT

The authors would like to thank A. A. Mouche from IFREMER for the provision of the empirical geophysical model function CDOP and appreciate the help given by him.

REFERENCES

[1] G. S. E. Lagerloef, G. T. Mitchum, R. B. Lukas, and P. P. Niiler, "Tropical Pacific near-surface currents estimated from altimeter, wind, and drifter data," *J. Geophys. Res. Oceans*, vol. 104, no. C10, pp. 23313–23326, Oct. 1999.

[2] P. Baynes, K. Dumper, C. Gommenginger, S. Gleason, and C. Mutlow, *Ocean Currents From Space*, document SOS-OC-REP-2/01, BNSC SMS Programme, 2002.

[3] P. Fabry *et al.*, "Feasibility study of sea surface currents measurements with Doppler scatterometers," *Currents*, vol. 240, pp. 50–100, Sep. 2013.

[4] R. L. Bernstein, G. H. Born, and R. H. Whritner, "SEASAT altimeter determination of ocean current variability," *J. Geophys. Res. Oceans*, vol. 87, no. C5, pp. 3261–3268, Apr. 1982.

[5] B. Chapron, F. Collard, and F. Ardhuin, "Direct measurements of ocean surface velocity from space: Interpretation and validation," *J. Geophys. Res. Oceans*, vol. 110, no. C7, pp. 691–706, Jul. 2005.

[6] R. Romeiser *et al.*, "Direct surface current field imaging from space by along-track InSAR and conventional SAR," in *Oceanography From Space*. New York, NY, USA: Springer, 2010, pp. 73–91.

[7] F. Fois, P. Hoogeboom, F. Le Chevalier, A. Stoffelen, and A. Mouche, "DopSCAT: A mission concept for simultaneous measurements of marine winds and surface currents," *J. Geophys. Res. Oceans*, vol. 120, no. 12, pp. 7857–7879, Dec. 2015.

[8] F. Fois, P. Hoogeboom, F. Le Chevalier, and A. Stoffelen, "DOPSCAT: A mission concept for a Doppler wind-scatterometer," in *Proc. IEEE Int. Geosci. Remote Sens. Symp.*, Jul. 2015, pp. 2572–2575.

[9] Q. Bao, X. Dong, D. Zhu, S. Lang, and X. Xu, "The feasibility of ocean surface current measurement using pencil-beam rotating scatterometer," *IEEE J. Sel. Topics Appl. Earth Observ. Remote Sens.*, vol. 8, no. 7, pp. 3441–3451, Jul. 2015.

[10] B. Qingliu, D. Xiaolong, and Z. Di, "Ocean surface current measurement using pencil-beam rotating scatterometer," in *Proc. IEEE Geosci. Remote Sens. Symp. (IGARSS)*, Jul. 2014, pp. 684–687.

[11] W. J. Pierson, Jr., "Probabilities and statistics for backscatter estimates obtained by a scatterometer," *J. Geophys. Res. Atmos.*, vol. 94, no. C7, pp. 9743–9759, Jul. 1989.

[12] C. Y. Chi and F. K. Li, "A comparative study of several wind estimation algorithms for spaceborne scatterometers," *IEEE Trans. Geosci. Remote Sens.*, vol. GRS-26, no. 2, pp. 115–121, Mar. 1988.

[13] A. Stoffelen and M. Portabella, "On Bayesian scatterometer wind inversion," *IEEE Trans. Geosci. Remote Sens.*, vol. 44, no. 6, pp. 1523–1533, Jun. 2006.

[14] M. Portabella and A. Stoffelen, "A probabilistic approach for SeaWinds data assimilation," *Quart. J. Roy. Meteorol. Soc.*, vol. 130, no. 596, pp. 127–152, Jan. 2004.

[15] M. W. Spencer, C. Wu, and D. G. Long, "Improved resolution backscatter measurements with the SeaWinds pencil-beam scatterometer," *IEEE Trans. Geosci. Remote Sens.*, vol. 38, no. 1, pp. 89–104, Jan. 2000.

[16] J. N. Huddleston and M. W. Spencer, "SeaWinds: The QuikSCAT wind scatterometer," in *Proc. IEEE Aerosp. Conf.*, Mar. 2001, pp. 1825–1831.

[17] X. Jiang *et al.*, "The HY-2 satellite and its preliminary assessment," *Int. J. Digit. Earth*, vol. 5, no. 3, pp. 266–281, 2012.

[18] E. Rodriguez *et al.*, "Ka-band Doppler scatterometer for measurements of ocean surface vector winds and currents," presented at the Earth Sci. Technol. Forum, Los Angeles, CA, USA, 2014.

[19] A. Stoffelen and D. Anderson, "Scatterometer data interpretation: Measurement space and inversion," *J. Atmos. Ocean. Technol.*, vol. 14, no. 6, pp. 1298–1313, 1997.

[20] M. Portabella, "Wind field retrieval from satellite radar systems," Ph.D. dissertation, Dept. Astron. Metereol., Univ. Barcelona, Barcelona, Spain, 2002.

[21] M. H. Freilich. (2000). *SeaWinds Algorithm Theoretical Basis Document*. [Online]. Available: http://eospso.nasa.gov/sites/default/files/atbd/atbd-sws-01.pdf

[22] W. Lin, "Study on spaceborne rotating, range-gated, fanbeam scatterometer system," Ph.D. dissertation, Dept. Comput. Appl. Technol., Center Space Sci. Appl. Res., Chin. Acad. Sci., Beijing, China, 2011.

[23] R. Romeiser and D. R. Thompson, "Numerical study on the along-track interferometric radar imaging mechanism of oceanic surface currents," *IEEE Trans. Geosci. Remote Sens.*, vol. 38, no. 1, pp. 446–458, Jan. 2000.

[24] F. Fois, P. Hoogeboom, F. Le Chevalier, and A. Stoffelen, "An analytical model for the description of the full-polarimetric sea surface Doppler signature," *J. Geophys. Res. Oceans*, vol. 120, no. 2, pp. 988–1015, Feb. 2015.

[25] A. A. Mouche, B. Chapron, N. Reul, and F. Collard, "Predicted Doppler shifts induced by ocean surface wave displacements using asymptotic electromagnetic wave scattering theories," *Waves Random Complex Media*, vol. 18, no. 1, pp. 185–196, 2008.

[26] A. A. Mouche *et al.*, "On the use of Doppler shift for sea surface wind retrieval from SAR," *IEEE Trans. Geosci. Remote Sens.*, vol. 50, no. 7, pp. 2901–2909, Jul. 2012.

[27] M. S. Longuet-Higgins, D. Cartwright, and N. Smith, "Observations of the directional spectrum of sea waves using the motions of a floating buoy," in *Proc. Conf. Ocean Wave Spectra*, 1963, pp. 111–136.
[28] J. R. Apel, "An improved model of the ocean surface wave vector spectrum and its effects on radar backscatter," *J. Geophys. Res., Oceans*, vol. 99, no. C8, pp. 16269–16291, Aug. 1994.
[29] D. G. Long and G. B. Skouson, "Calibration of spaceborne scatterometers using tropical rain forests," *IEEE Trans. Geosci. Remote Sens.*, vol. 34, no. 2, pp. 413–424, Mar. 1996.
[30] Q. Bao, "System design and simulation of Doppler scatterometer—Wide swath ocean surface current measurement," Ph.D. dissertation, Dept. Electromagn. Field Microw. Technol., Univ. Chin. Acad. Sci., Beijing, China, 2015.

Qingliu Bao was born in Hebei, China, in 1986. He received the B.S. degree in electrical engineering from Xidian University, Xi'an, China, in 2010, and the Ph.D. degree in engineering from the University of Chinese Academy of Science, Beijing, China, in 2015.

He is currently a Post-Doctoral Fellow with the National Satellite Ocean Application Service, SOA, Beijing, and also with the Center for Earth System Science, Tsinghua University, Beijing.

His research interests include the microwave remote sensing of ocean, the system design and signal processing of scatterometer data, ocean surface wind and current field inversion.

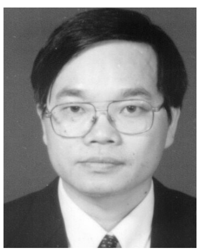

Mingsen Lin was born in Fujian, China, in 1963. He received the B.E. degree in applied mechanics from the National University of Defense Technology, Changsha, China, in 1984, and the Ph.D. degree from the Chinese Academy of Sciences, Beijing, China, in 1992.

From 1992 to 1994, he was a Post-Doctoral Research Fellow and an Associate Professor with Tianjin University, Tianjin, China. From 1994 to 1999, he was with the Third Institute of Oceanography, State Oceanic Administration, Xiamen, China, as an Associate, Research Fellow, a Research Fellow, and the Departmental Director successively. He was the Founder of satellite ocean remote sensing in China, and performed an important role in the development of the Chinese Ocean Satellite and Manned Space Flight. He was the Deputy Chief Designer of ground application system for HY-1 and HY-2 satellites, where he organized the argument of the Chinese Ocean Satellite outline, and managed the construction of ground application system for the Chinese Ocean Satellite. In 1999, he joined the National Satellite Ocean Application Service, State Oceanic Administration, Beijing, where he is currently the Senior Scientist and the Deputy Director. He has acquired the special government allowance since 1998. His research interests include the remote sensing of the ocean and computation fluid dynamics.

Prof. Lin was awarded as the JCOMM-OPA ocean and meteorological satellite expert and the CEOS ocean topography expert in 2006. He has been the Two Hundred Talents Professor of the State Oceanic Administration since 1997, and was selected as the first level talent of the National Talents Project in 1998.

Youguang Zhang was born in Shandong, China, in 1971. He received the Ph.D. degree in oceanography from the Institute of Oceanology, Chinese Academy of Sciences, Qingdao, China, in 2004.

He was with the National Satellite Ocean Application Service (NSOAS), State Oceanic Administration, Beijing, China, since 2004, where he is currently a Research Fellow and the Departmental Director. He is also the Chief Designer of ground application system for HY-2 and CFOSAT, and in charge of the construction of their subsystems. He has hosted and taken part in more than 30 projects, such as Manned Flight Project, Marine Public, 863 Project, and National Research and Development Plan. He has authored or co-authored more than 50 papers. His research interests include the microwave remote sensing of the ocean, data processing, and the calibration of active microwave remote sensors, satellite ground application system construction, and the advanced research of new type ocean remote sensing payloads.

Xiaolong Dong was born in Shaanxi, China, in 1969. He received the B.E. degree in radio technology and the Ph.D. degree in electromagnetic theory and microwave techniques from Xi'an Jiaotong University, Xi'an, China, in 1991 and 1996, respectively.

From 1996 to 1999, he was a Post-Doctoral Research Fellow and an Associate Professor with the National Space Science Center, Chinese Academy of Sciences, Beijing, China, and then promoted as a Full Professor in 1999. From 2001 to 2003, he was with Duke University, Durham, NC, USA. Since 2003, he has been a Hundred Talents Professor of the Chinese Academy of Sciences (CAS), National Space Science Center, Beijing, where he is currently the Director General of the Center and the Director of the CAS Key Laboratory of Microwave Remote Sensing. He has been a Principal Investigator of the scatterometers of several Chinese oceanic observation satellites, including the Chinese-French Oceanic Satellite and the Haiyang-2 satellite. He has authored or co-authored more than 80 journal papers and conference presentation. His research interests include the theory and techniques of microwave remote sensing, the development of advanced microwave sensors, with emphasis on radar scatterometry for atmospheric, oceanic, and land surface applications.

Shuyan Lang received the M.Eng. degree in electromagnetic field and microwave technology from the Center for Space Science and Applied Research, Chinese Academy of Sciences, and the Graduate University of Chinese Academy of Sciences, Beijing, China, in 2008.

Since 2008, she has been with the National Satellite Ocean Application Service, State Oceanic Administration, Beijing. Her research interests include the fields of data processing of scatterometer, and ocean remote sensing.

Peng Gong received the B.S. and M.S. degrees in geography from Nanjing University, Nanjing, China, in 1984 and 1986, respectively, and the Ph.D. degree in geography from the University of Waterloo, Waterloo, ON, Canada, in 1990.

He was a Research Scientist with the Institute for Space and Terrestrial Science, Toronto, ON, Canada, and an Assistant Professor with the Department of Geomatics Engineering, University of Calgary, Calgary, AB, Canada. He joined the Department of Environmental Science, Policy and Management, University of California, Berkeley, CA, USA, in 1994, where he became a Full Professor in 2001. He was the Advisor to the Ministry of Science and Technology of China from 2004 to 2006, the Founding Director of the International Institute for Earth System Science, Nanjing University, from 2000 to 2007, and the Founding Director of the State Key Laboratory of Remote Sensing Science, Chinese Academy of Sciences (CAS), and Beijing Normal University, Beijing, China, from 2004 to 2010. He joined the Center for Earth System Science, Tsinghua University, Beijing, as the Director in 2010. He has authored or co-authored six books and more than 360 journal articles in the field of remote sensing, geography, and environmental science. His research interests include remote sensing, global environmental change, and planetary health.

Prof. Gong received a number of honors and awards including the Outstanding Contribution Award in remote sensing from the Association of American Geographers in 2008 and the Talbert Abrams Grand Award from the American Society for Photogrammetry and Remote Sensing in 1994.